Computers and Electronics in Agriculture 150 (2018) 364–373

Contents lists available at ScienceDirect

Computers and Electronics in Agriculture

journal homepage: www.elsevier.com/locate/compag

Original papers

Development and characterization of a highly sensitive fluorometric transducer for ultra low aqueous ammonia nitrogen measurements in aquaculture

Cong Wang[a,b,c], Zhen Li[a,b,c], Zhongli Pan[d,e], Daoliang Li[a,b,c,*]

[a] College of Information and Electrical Engineering, China Agricultural University, Beijing 100083, China
[b] Key Laboratory of Agricultural Information Acquisition Technology, Ministry of Agriculture, Beijing 100083, China
[c] Beijing Engineering and Technology Research Centre for Internet of Things in Agriculture, Beijing 100083, China
[d] Healthy Processed Foods Research Unit, USDA-ARS-WRRC, 800 Buchanan St., Albany, CA 94710, USA
[e] Department of Biological and Agricultural Engineering, University of California, Davis, One Shields Avenue, CA 95616, USA

ARTICLE INFO

Keywords:
Ammonia nitrogen
Fluorescence
Pseudo-random sequence
Synchronous demodulation

ABSTRACT

The accurate measurement of ammonia nitrogen concentration is of great significance for the study of aquatic ecological processes. Unfortunately, the commonly used colorimetric and ammonia sensitive electrode methods suffer from poor consistency, especially when the concentration of ammonia nitrogen is low. This paper presents the development and characterization of a highly sensitive fluorometric transducer, intended for measuring ultra-low ammonia nitrogen concentration in natural waters. The design of the transducer is based on molecular fluorescence analysis and focused on the ammonia-orthophthaldialdehyde-sulfite complexation reaction in alkaline aqueous solutions. LED excitation and photodiode detection are integrated in a compact pressure hull, with a small dichroic beam-splitter installed on the optical path. The beam-splitter reflects a small percentage of ultraviolet light into the reference photodiode to evaluate variations of the excitation energy and simultaneously guide fluorescence light into the sample photodiode by total internal refection. As a major innovation, pseudo-random sequence modulation and self-calibration are introduced into the amplitude measurement of the fluorescence for the first time. Specifications include a limit of detection (LOD) of 0.16 $\mu g \cdot L^{-1}$, a measurement range of 0–419.31 $\mu g \cdot L^{-1}$, and the R-square of 0.99. Two sets of algorithms with inputs of pH, temperature, salinity, and atmospheric pressure are embedded into the device for the high-precision measurement.

1. Introduction

Ammonia nitrogen refers to ammonia in natural waters in the form of free ammonia (NH_3) or ammonium salt (NH_4^+) (Zhang et al., 2018). The composition proportion of ammonia depends on the pH and temperature of water. When the pH value is high, the proportion of free ammonia is higher. On the contrary, the ratio of ammonium salt is higher. The effect of water temperature is the opposite (Mooney et al., 2018).

With the rapid development of aquaculture, the usage of high-yield and high-density aquaculture is increasing swiftly, and the pollution of aquaculture water bodies is becoming more and more dire (Eshchar et al., 2006; Hoang et al., 2017). Aquaculture water often brings about the deterioration of water quality because of the corruption and decomposition of residue, chemical and therapeutic drug residues, aquatic biological excreta and corpses in the pool (Ben-Asher and Lahav, 2016). It causes abnormal changes of nitrogen and phosphorus in water, and produces harmful substances, such as ammonia nitrogen, nitrite and more, inducing fish, shrimp and other breeding objects to attack or even die (Lich and Kumar, 2017; Ardeniswan and Sukmawati, 2017) , which greatly hampers the development of aquaculture. Because of the influence of human activities, the content of ammonia nitrogen in the water is high (Li et al., 2017; Hou et al., 2017), even to the degree of poisoning the aquatic organisms and destroying the ecological balance of the water body (Zhou and Boyd, 2015). When the concentration of ammonia nitrogen in the river is too high, the chlorine used in drinking water will be consumed by ammonia nitrogen, resulting in poor disinfection of drinking water (Ding et al., 2016; Zhang, 2017; Mook et al., 2012). Furthermore, the ammonia nitrogen in drinking water can be easily transformed into nitrate (Zhang et al., 2016), which will poison the human body.

Ammonium nitrogen is an important component of dissolved

* Corresponding author at: College of Information and Electrical Engineering, China Agricultural University, Beijing 100083, China.
E-mail address: dliangl@cau.edu.cn (D. Li).

https://doi.org/10.1016/j.compag.2018.05.011
Received 4 February 2018; Received in revised form 3 May 2018; Accepted 8 May 2018
Available online 14 May 2018
0168-1699/

inorganic nitrogen in seawater (Ma et al., 2014; Yu et al., 2017). Its content is affected by biological metabolism, nitrate and nitrite reduction, and exchange of air-sea interface and seawater sediment interface (Cheng et al., 2015; Rixen et al., 2014; Johnson et al., 2008). Under the irradiation of ultraviolet light, natural dissolved organic matter decomposes and releases ammonium. This process of ammonium generation under ultraviolet irradiation is called photoammonification (Bushaw et al., 1996). In recent years, the effect of light ammoniation as a source of active nitrogen in water environment and its role in the nitrogen cycle has been paid more and more attention. Accurate determination of micro-ammonium content in the process of photo ammoniation is of great importance for correctly understanding the nitrogen cycle, evaluating eutrophication in the seas and revealing the processes involved in marine ecology.

A number of methods exist for measuring ammonium (Hong and Rhee, 2014; Hashihama et al., 2015; Zhu et al., 2014; Strobl et al., 2017). When culture water containing more organic matter is determined by the sodium hypobromite oxidation method (Zhou, 2016; Guan et al., 2017), the error is larger and the blank value of the aquaculture water is high, which will cause serious interference. Nessler's reagent colorimetric method (Kołacińska and Koncki, 2014; Zeng et al., 2014) is a classical method for the determination of ammonia nitrogen and is listed as a standard method in many countries. Its disadvantage is that the reagents used are highly toxic. In addition, calcium, magnesium and other metal ions, sulfides, aldehydes and ketones, colors, and turbidity will interfere with the determination. The salicylate method is another colorimetric method (Cho et al., 2018); the interference and elimination of this method are the same as in Nessler's reagent colorimetric method. When ammonia nitrogen is detected by the Ammonia Gas-sensitive Electrode method (Naidji et al., 2016), the color and turbidity of the water sample have no influence on the measurement system. Therefore, water samples are usually not required to be pretreated. Moreover, the detection method needs fewer reagents, and has simple operation and a wide measurement range. It is fast, sensitive and reliable, and it meets the requirements of environmental analysis (Mueller and Hemond, 2016). However, the detection limit (LOD) of the method is high (ca.100 $\mu g \cdot L^{-1}$), and it can easily be influenced by a high concentration of ions (Zhang et al., 2014). When the organic components are included in the solution, they will have a great effect on the results of the determination. In addition, there are still some problems with the lifespan and reproducibility of the ammonia gas sensitive electrode.

The method that we present here is an adaptation of a recently published continuous-flow fluorometric technique (Horstkotte et al., 2011; Valente et al., 2017; Šraj et al., 2014; Liang et al., 2016). Our modified method optimizes analysis of samples with a measurement range of 0–419 $\mu g \cdot L^{-1}$, a limit of detection (LOD) of 0.16 $\mu g \cdot L^{-1}$ and self-calibration. Unlike other fluorometric analysis methods, only one fluorescent probe is required for this detection method, and no special HPLC separation (Hu et al., 2014a, 2014b, 2014c; Dahlberg et al., 2015; Matsui et al., 2010) or flow injection devices (Ohira et al., 2013; Šraj et al., 2014) are needed. We begin by discussing the mathematical model for ultra-weak light detecting method. Next, details of the transducer design considerations as well as the design of fluorescence measurement electronics are presented. We then report the solutions preparation, as well as the basic experimental procedure. Finally, the fluorometric transducer is analyzed from the aspect of reproducibility, salinity effects and accuracy, and the calculation of unionized ammonia is supplemented.

2. Mathematical model for Ultra-weak light detecting method

The single frequency modulation method is the basic solution for ultra-low noise precision measurements (Jiménez-Márquez et al., 2015; Xin et al., 2011; Akbarzadeh-Jahromi and Shahabadi, 2017). The key of this method is that the emission signal is at the same frequency as the modulated excitation signal. Because ambient light interference exists at low frequency, the emission signal can easily be extracted from the interference through a high pass filter in the frequency domain. This technology has been very popular in recent years and is often used in some online optical sensors to improve the accuracy of detection (Hu et al., 2014a, 2014b, 2014c; Yang et al., 2010).

However, once the modulated emission signal falls into the same frequency band as the high order harmonic interference caused by the electromagnetic environment, the accuracy of the transducer will be reduced (Hu et al., 2013). To further reduce noise by improving the signal-to-noise ratio (SNR) of the measured signal, the following weak light detection methods may be useful (Zhang et al., 2009). A light chopping wave phase-locked amplifier and periodic signal detection, using a sampling integrator and photon counting device based on cumulative average method, may improve the SNR of the output signal. In addition, wavelet analysis and chaos theory are also used to detect weak electrical signals.

Pseudo random sequence (PRS), another modulation technique (Roinila et al., 2016; Pan et al., 2011), is a binary sequence with good randomness, many of its characteristics are close to white noise, and it can be generated by the determined method (Lukin and Shcherbakov, 2016). The pseudo random sequence has been applied in many fields. In this paper, a method of detecting the ultra-weak signal amplitude by using the strong autocorrelation property of pseudo random sequence is presented.

The principle of PRS correlation detection is shown in Fig. 1. A pseudo random sequence $P(t)$ is generated by a feedback shift register circuit or microprocessor circuit. At almost the same time that the PRS modulates the light source, the emission signal goes to the receiving end of the measurement system. The optical output signal $x(t)$ is obtained after photoelectric conversion, signal filtering and amplification. According to Lambert-Beer's law (Mayerhöfer et al., 2016), for a dilute

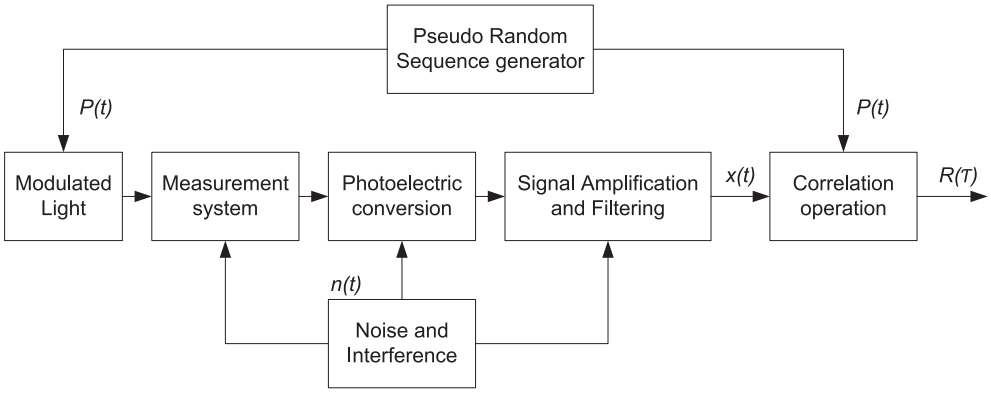

Fig. 1. Mathematical model for correlation detection of pseudo-random sequence.

Table 1
Symbols and Significations in Expression (1).

symbol	Significations
$I_f(t)$	Fluorescence intensity in time domain
Y_f	Quantum yield of fluorescence
I_o	Incident light intensity driven by constant current
ε	Mole absorption coefficient of fluorescent molecules
b	Thickness of sample pool
c	The concentration of a fluorescent substance in a solution

solution of a fluorescent substance (see Table 1),

$$I_f(t) = 2.3Y_f I_0 P(t)\varepsilon bc \tag{1}$$

The signal $x(t)$ can be simplified as

$$x(t) = G[I_f(t) + n(t)] = G[KcP(t) + n(t)] \tag{2}$$

where G is the gain constant of the transducer, K is the total instrument constant, and $n(t)$ represents the noise and interference. The signal $x(t)$ and sequence $P(t)$ perform a cross-correlation operation,

$$\begin{aligned} R_{xp}(\tau) &= \lim_{T\to\infty} \tfrac{1}{T}\int_0^T x(t)p(t-\tau)dt = GKcR_{pp}(\tau) + GR_{np}(\tau) \\ R_{pp}(\tau) &= \lim_{T\to\infty} \tfrac{1}{T}\int_0^T p(t)p(t-\tau)dt = \delta(\tau) \\ R_{np}(\tau) &= \lim_{T\to\infty} \tfrac{1}{T}\int_0^T n(t)p(t-\tau)dt \end{aligned} \tag{3}$$

where R_{pp} is an autocorrelation function of PRS, R_{np} is a cross-correlation function of PRS and the noise-interference signal, and $\delta(t)$ represents the pulse function. Because the PRS is not related to noise or interference,

$$R_{np}(\tau) = 0 \tag{4}$$

Thus, the cross-correlation function R_{xp} can be simplified to

$$R_{xp}(\tau) = GKc\delta(\tau) \tag{5}$$

The formula (5) indicates that the peak of the measured cross correlation function is the intensity of the weak signal mixed in the noise.

3. Experimental details

3.1. Transducer design considerations

The principal optical configuration is shown in Fig. 2. The miniature fluorometric transducer can be used to analyze the concentration of ammonia in aqueous solutions by measuring the amount of isoindole derivatives' (reaction products of ammonia nitrogen and ortho-phthalaldehyde) fluorescence (Yan et al., 2015) emissions from a given sample volume. The isoindole derivatives, when excited by an external light source, absorb light in certain regions of the visible spectrum (mainly in 365 nm ultraviolet light) and re-emit a small portion of the absorbed energy as fluorescence at longer wavelengths around 430 nm (Hu et al., 2014a, 2014b, 2014c).

The fluorometric transducer uses one ultra-bright UV LED in a pseudo-random sequence modulation mode to provide the excitation light. A small dicroitic beam-splitter (short wave pass, LWP) is used to reject the small amount of blue-violet light emitted by the LED. The small percentage of UV light which is also reflected by the dicroitic beam-splitter is used as a reference signal to evaluate variations of the excitation energy. A temperature sensor installed on the back of the reference photodiode monitors the body temperature of the photodiode in real time, and the monitoring value can be used to assess the impact of the chip's temperature drift on photoelectric conversion. Internal reference measurements of the emitted light compensate for aging and temperature dependencies of the high-efficiency LED, used for fluorescence excitation.

The excitation beam is focused approximately 15 mm in front of the artificial corundum window by a small lens. Fluoresced light is collected by the same lens, reflected by a dicroitic beam-splitter and detected by a large area photodiode. A violet interference filter is used in front of the photodiode to discriminate stray-light. Apart from the optoelectronics, three compact circuit boards are also housed in the probe.

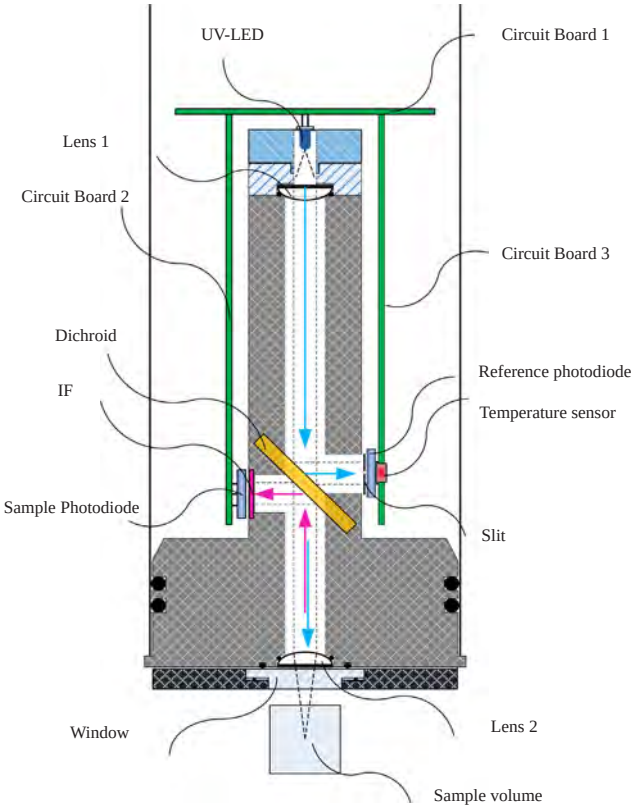

Fig. 2. Optical layout of Fluorometric transducer.

3.2. Fluorescence measurement electronics and data acquisition

A PRS based on a MCU (MSP430F149) generates as shown in Fig. 3. Here, we select m-sequence (N = 32, T = 1/4096 s) as the modulation and demodulation signal, which is the most widely used and mature PRS. The determined sequence can be burned to the memory of the MCU by programming. The MCU built-in timer sets the basic code width, triggers the MCU kernel to read the sequence values from the memory, and controls the IO port of the MCU to output modulation sequence.

The circuit of the excitation module is shown in Fig. 4. It is composed of a Field Effect Tube (IRLL014) and a series of current limiting resistors. A low-cost LED (YCL-UV360-370, ShenZhen YuanChuang Electronic Co. Ltd., China) delivers a radiated power of 12 mW at a wavelength of 365 nm. We drive the LED intensity with a style of pseudo random sequence modulation.

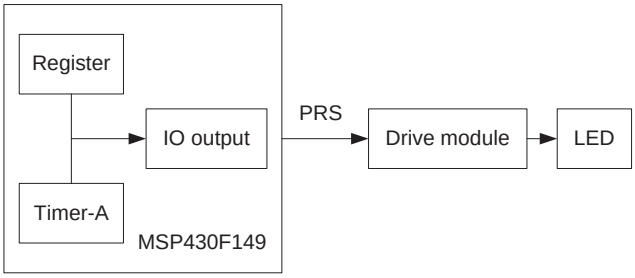

Fig. 3. Pseudo-random sequence generator module.

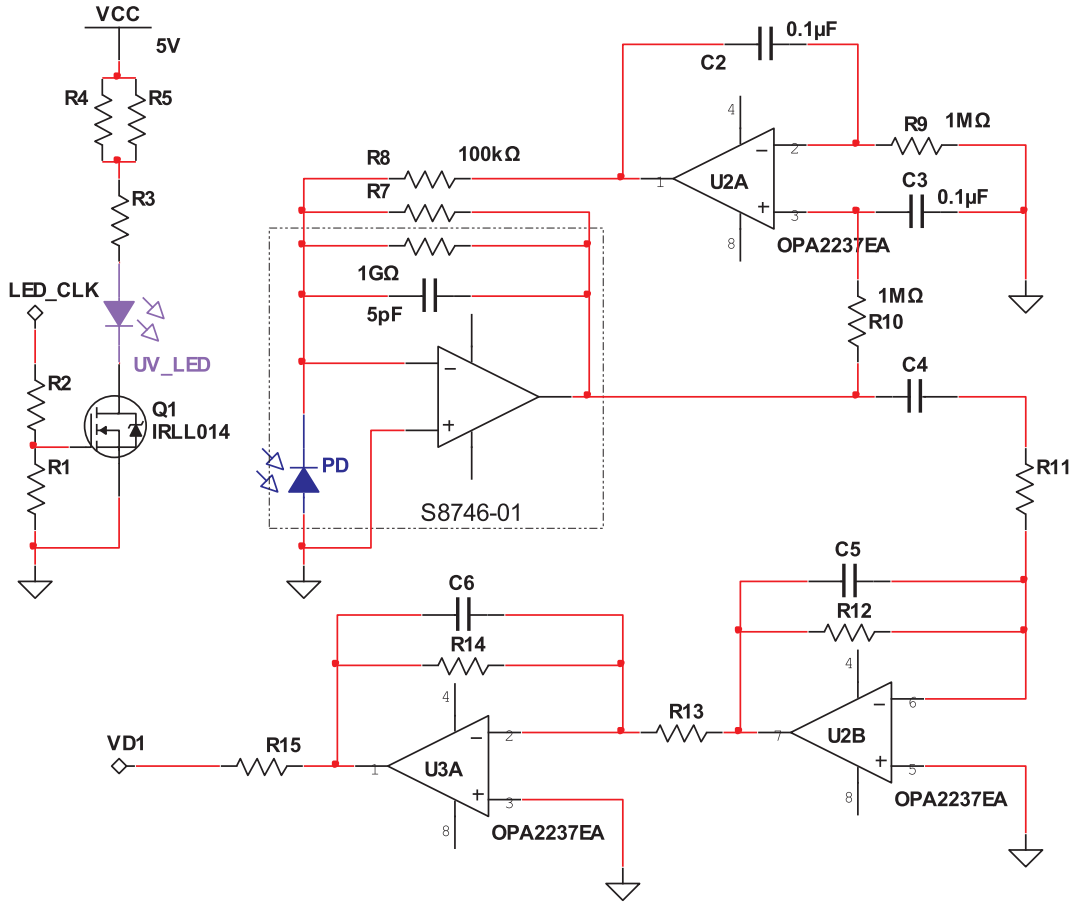

Fig. 4. LED driver circuit and photodiode-amplifier with DC restoration rejects unwanted background light.

In Fig. 4, a specially developed circuitry eliminates the influence of ambient light, which is normally present in surface waters. The circuit uses the S8746-01 (Hamamatsu Photodiode) integrated photodiode and amplifier and external op amps (U2A) for DC (constant current) restoration. The S8746-01 combines a large 5.8 × 5.8 mm photodiode and high-performance transimpedance amplifier on a single chip. This combination eliminates the problems commonly encountered in discrete designs such as leakage current errors, noise pick-up, and gain peaking due to stray capacitance. The DC restoration circuit consists of a non-inverting integrator driving the S8746-01 transimpedance amplifier summing junction through a 1MΩ resistor, R8. The current through R8 cancels the current from the photodiode at signal frequencies below the pole frequency of the integrator to drive the output of the S8746-01 to 0 V. The pole-frequency of the integrator is set by R9 and C2.

$$f_{-3dB} = \frac{1M}{R_8(2\pi R_9 C_2)} \tag{6}$$

The component values shown in Fig. 4 set the low frequency cutoff pole at 16 Hz. Because of the long time constant, it may take over a second for the S8746-01 output to come out of saturation when the circuit is first powered-up.

A non-inverting integrator requires a matching pole. The matching pole, set by R10 and C3, prevents the S8746-01 output signals above the pole frequency from feeding directly back into the summing junction of the S8746-01. The value used for R8 depends on the amplitude of the background light. With 10 V output on S8746-01, the 100kΩ resistor can provide 100uA restoration current to the photodiode. This is one hundred times the photodiode current that would otherwise drive the S8746-01 to 10 V output when using the external 10MΩ resistor, R7. The DC restoration circuit can remove a background signal many times larger than the AC signal of interest providing the increased critical signal-to-noise level in many applications. Reducing the value of R8 will increase the DC restoration range, but it will also increase the noise gain of the transimpedance amplifier. Values above 100kΩ for R8 will not substantially reduce noise.

The fluorescence signal of low concentration detection is very weak, so after first stage amplification and filtering, it needs to be magnified many times before demodulation. The amplifier (U2B) input terminal has an AC coupling circuit, which only allows the AC signal to pass through, further filtering out the DC and low frequency signals.

According to Lambert-Beer's law, the intensity of the fluorescence signal detected by the detector has a negative exponential relationship with the product of the intensity of the excitation source and the substance concentration. LEDs are the most commonly used excitation sources. The luminous stability and efficiency of LEDs are related to the working temperature and time of LEDs. With aging or the increase of temperature, their luminous efficiency will decrease (Li et al., 2015). Based on the characteristics, a sensor self-calibration method is proposed in this paper. The output voltage of the transmitter is corrected in real time by monitoring the fluctuation of the excitation light through the reference light path, and the temperature drift of the photodiode in the reference light path is compensated by a linear temperature sensor (TMP01). The reference monitoring circuit is similar to the fluorescence signal amplification and filtering circuit in Fig. 4.

$$K = V_{set}/[V_R - \alpha G(t - 25°C)]$$
$$V_f = KV_o \tag{7}$$

where K is the transmitter correction factor, V_{set} records the initial light intensity of UV-LED in the factory calibration (25 °C), V_R records the light intensity of UV-LED in the actual work, α is the temperature drift

coefficient of the reference photodiode (S8746-01) under the condition of 365 nm wavelength, t is the working temperature of the reference photodiode, G is I-V amplification gain in the reference circuit, V_o is the fluorescence intensity that the transducer actually reads, and V_f is the corrected fluorescence intensity.

It is known from the autocorrelation of the pseudo-random sequence modulation that the signal demodulation must be strictly synchronized to restore the fluorescence signal. VD1 and VD2 are the fluorescence and the reference light output signals after two stages of amplification and filtering respectively, as shown in Fig. 4. The demodulation circuit is composed of an analog switch, two differential amplifier circuits and a phase shift circuit. The MAX4674 is a low-voltage CMOS analog switch containing four 2:1 multiplexers/demultiplexer. When powered from a single +5 V supply, it features a low 4Ω max on-resistance (R_{ON}), 0.4 Ω max R_{ON} matching between channels, and 0.8 Ω R_{ON} flatness over the entire signal range. Off-leakage current is only 0.5 nA max at 25 °C. The MAX4674 features fast turn-on and turn-off times of 18 ns and 6 ns, respectively. It is suitable for low power, high frequency system applications.

In our design, the demodulation signal (LED_CLK) is controlled by the timer-A output as well as the excitation light modulation signal, but there may be a phase difference between the demodulated signal VD1/VD2 and the demodulation signal (SYNCH_CLK). The filter parameters (U6A, R22-R26, and C10) can be adjusted to make them achieve complete synchronization.

It is shown in Fig. 5 that this is actually an absolute value detection circuit based on zero point potential, but because of the existence of a synchronous signal, it is also equivalent to synchronous demodulation of fluorescence and demodulation signals by multiplication. The synchronization demodulation scheme has high frequency selectivity, and it can extract the output signal of the first three stages of amplification and filtering. After the demodulated signal VD1/VD2 are smoothed through two low pass filters composed of R29-R30-C8 and R38-R39-C9, two stabler DC signals together with one temperature signal are then sent into a low power, low noise, 16-bit sigma-delta analog to digital converter AD7798, with three differential analog inputs.

3.3. Materials and equipment

3.3.1. Solutions preparation

All solutions were prepared with freshly drawn ultrapure deionized (DI) water and analytical grade chemicals. The 1.85×10^4 μg·L^{-1} ammonium stock solution was prepared by adding 45.5 mL of 1.0×10^5μg·L^{-1} ammonia standard solution into 200 mL of DI water. The ortho-phthalaldehyde (OPA) solution was prepared by adding 2 g of OPA to 50 mL of high-grade ethanol (> 99.5%). OPA is light sensitive, so it should be protected from light while dissolving in ethanol and stored in the dark. The borate buffer solution was prepared by adding 40 g of sodium tetraborate to 1000 mL of DI water. In order to improve the sensitivity and stability of the fluorescent solution system, sodium sulfite was added to the fluorescence system as a stabilizer and sensitizer. The sodium sulfite solution was prepared by adding 2 g of sodium sulfite to 250 mL of DI water. All solutions were stirred or shaken thoroughly to dissolve. In a large (> 1000 mL), black, high-density polyethylene bottle, we mixed 5 mL of sodium sulfite solution, 1000 mL of borate buffer solution, and 50 mL of OPA solution as the working reagent. Ideally, allow the working reagent to “age” for 1 day or more

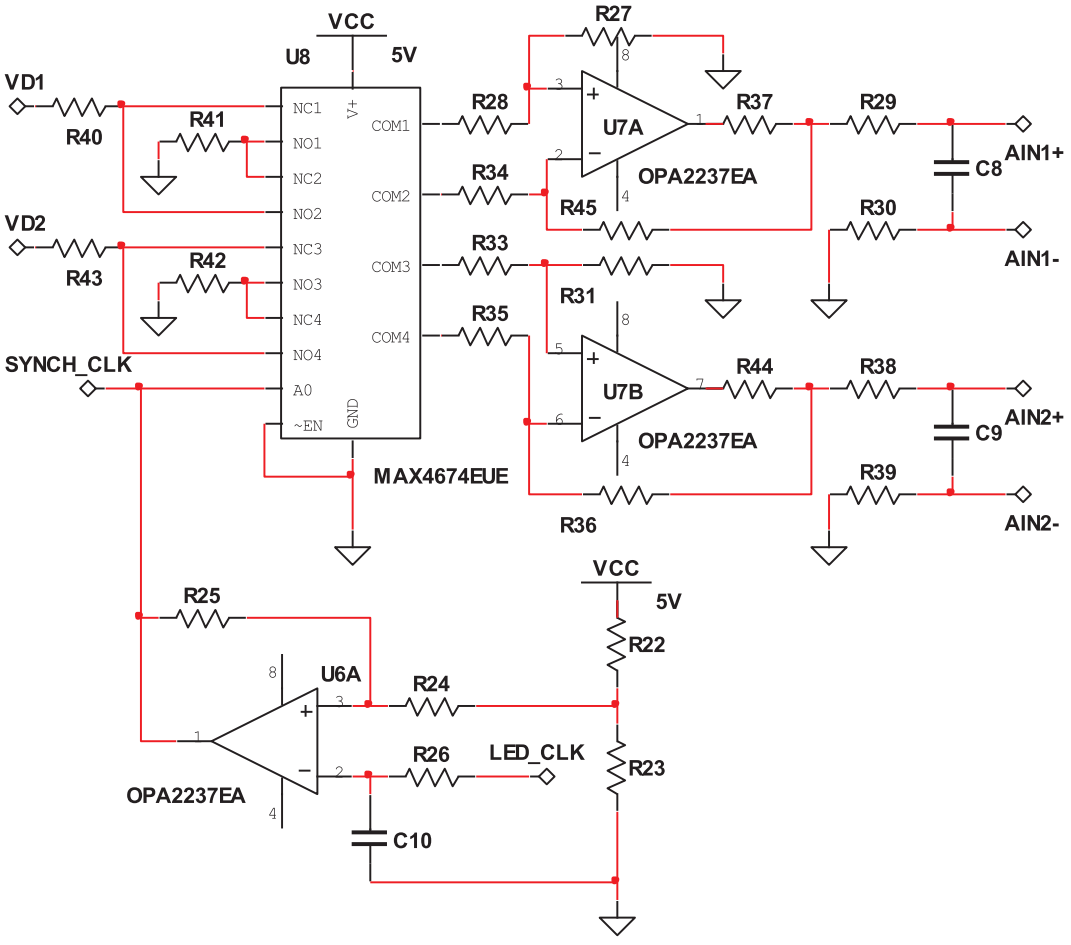

Fig. 5. Synchronous demodulation circuit.

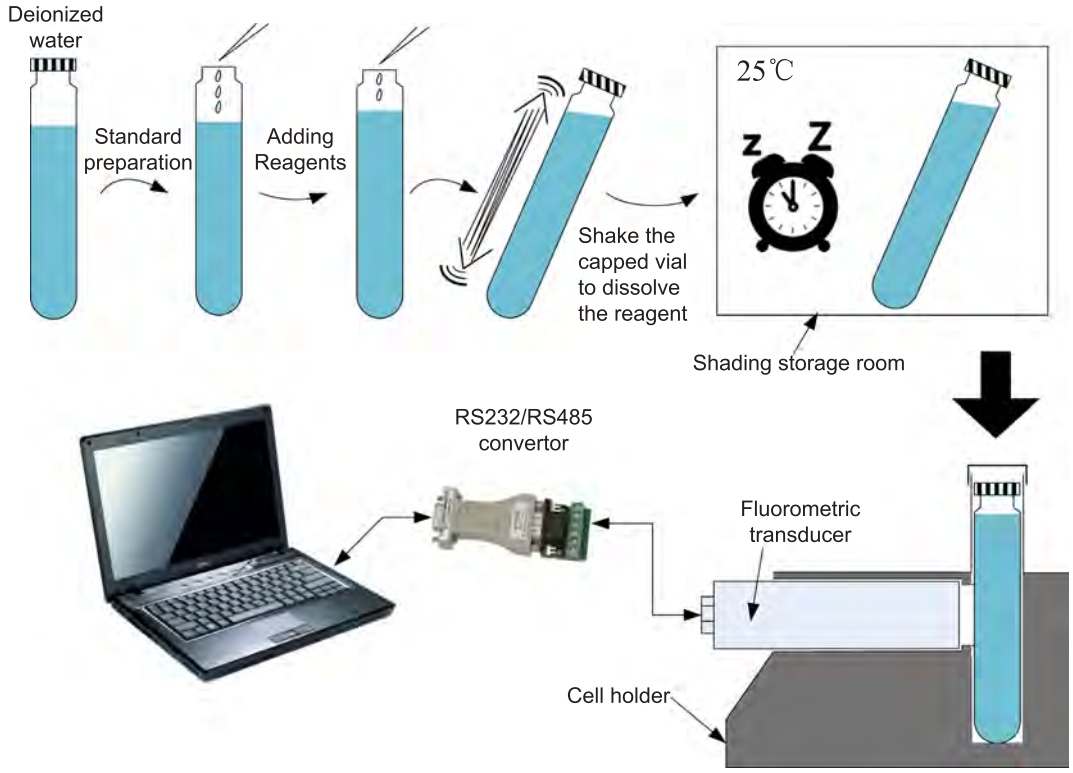

Fig. 6. Basic operation procedure.

in the dark prior to use because its blank will decrease over time.

3.3.2. Basic procedure

Fig. 6 shows an operation process of the experimental equipment used in this study. Take a set of capped vials to the analytical laboratory filled with precisely 10.5 mL of DI water. Carefully pipet 0–0.2 mL of ammonium stock solution and 1 mL of working reagent into each vial. Immediately shake the capped vial 10–20 times to dissolve the reagent in the vial, and store in the dark room (25 °C). After incubating for one reaction period, thoroughly clean the outside of the vial and insert the prepared vial into the cell holder. The transducer reads the fluorescence intensity of the reaction product and transfers the measured data to the master computer through a RS232/RS485 converter. It is important to note that, when the sensor calibration work is completed, the vial filled with 10.5 mL of DI water and a small amount of the ammonium stock solution needs to be replaced by 10.5 mL of samples before adding the working reagent.

3.4. Experimental set-up and results

3.4.1. Characterization of the reaction

To investigate the kinetics of the reaction, one standard solution (109.80 $\mu g \cdot L^{-1}$ ammonium) was prepared and measured at intervals over a 5-h period until the transducer output voltage was stable. Note that since the complexing reaction is sensitive to temperature and ambient light, the samples and working reagent should start in the dark at approximately the same room temperature (generally 25 ± 3 °C). The transducer read maximum fluorescence signal after 4 h and remained relatively stable for several more hours (Fig. 7). Ideally, the isoindole derivatives should be recorded during the time course of plateau, 4–5 h after mixing the working reagent and samples.

3.4.2. Calibration curve

Calibration experiments were carried out at room temperature. In order to measure the response of the transducer to different standard solution concentrations, we prepared 0, 17.60, 35.17, 52.71, 70.21, 87.68, 174.53, 260.56, and 345.79 $\mu g\,L^{-1}$ ammonium standards (Addition of 0, 0.2, 0.4, 0.6, 0.8, 1.0, 2.0, 3.0 and 4.0 mL of ammonium stock solution ($1.85 \times 10^4\ \mu g\,L^{-1}$) to 210 mL of DI water results in these standards. When calculating standard concentration, one must account for the volume of the stock solution added to the DI water.) in two hours and made a copy of each concentration in the first 2 days. Fig. 7 shows the relationship between the ammonium standards and the values read by the fluorometric transducer. Under the two experimental conditions, the linear regression effect of the transducer was very good, with little variability among days. Regression equations of the probe were calculated according to the principle of least squares, which were $y = 5.63x + 127.9$ and $y = 5.61x + 131.49$, and both correlation coefficients were $R^2 = 0.99$. There were no jump points. Results show that all the samples can be read by the inverse equation:

$$C_a = \lambda \times (V_f - B) \tag{8}$$

where C_a, is concentration of ammonia nitrogen in samples ($\mu g \cdot L^{-1}$), λ is transducer conversion coefficient ($\lambda = 2/(5.63 + 5.61) = 0.18\ \mu g \cdot L^{-1}$/mV), V_f is the corrected fluorescence intensity (mV), and B is signal strength of the reagent blank (B = (127.9 + 131.49)/2 = 129.70 mV).

3.4.3. Reproducibility of the transducer

The fluorometric transducer repeatability test was performed 75 times with three standard solution concentrations of 87.68, 174.53, and 345.79 $\mu g \cdot L^{-1}$ ammonium, and the measuring time was set to 20 s for each test. The results are shown in Fig. 8. From the test results, we observe that the photoinduced current (fluorescence signal channel) collected by the transducer fluctuated within 6.0×10^{-4} nA. The maximum relative deviation was 0.14%. It indicates that the fluorometric transducer has very high reproducibility.

3.4.4. Salinity effects, matrix effects

In order to study the effect of ionic strength on the fluorescence intensity of the reaction product, we made ammonia standard solutions

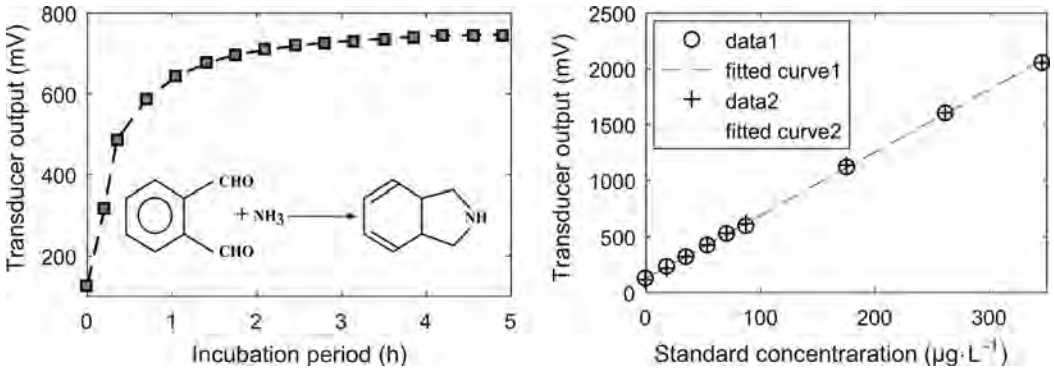

Fig. 7. Time course of the reaction and standard ammonia nitrogen calibration results.

by adding ammonium chloride crystal into artificial sea water with different salinities (10, 21.5, and 32.2 ppt). Twelve solutions consisting of four groups with different salinity standard solution concentrations of S1-52.71, S2-174.53, S3-260.56, and S4-345.79 $\mu g{\cdot}L^{-1}$ ammonium were prepared. The artificial seawater is based on Hiker Ocean Pro Sea Salt which is colorless, foamless, has no precipitation, is not muddy. More importantly, there is no nitrate, phosphate, ammonium or other toxic components. After incubating for 4 h, we put the probe into the home-made sample cell immediately. Concentration values were recorded every 20 s and sequentially measured five times. The average full scale precisions (± *%F.S) are shown in Fig. 9. The data analysis results indicate that the salinity in sea water has little influence on the isoindole derivatives.

Matrix effects are caused by substances in the sample that alter the intensity of the fluorescence caused by ortho-phthaldialdehyde (OPA) reacting with ammonium in the sample. The primary amines, including amino acids were investigated as potential sources of interference. Among the 16 compounds, such as urea, dimethylamine, glycine and leucine tested in seawater and freshwater, interferences never exceeded 0.5%, as observed by Kérouel and Aminot (Kérouel and Aminot, 1997).

Some common metal ions, anions may also alter the reaction. These are the copper, iron, and mercury. Additionally, the interference of sulfide, bromine, iodide and nitrate were tested at a level of 4 μ mol L^{-1} (56 $\mu g{\cdot}L^{-1}$) of ammonia (see Table 2).

Although matrix effects are often small (particularly when measuring in most natural waters), they can be substantial in some samples and must be considered. The prior work presented a method (Holmes et al., 1999) for dealing with matrix effects that allowed accurate correction of results by fluorometry.

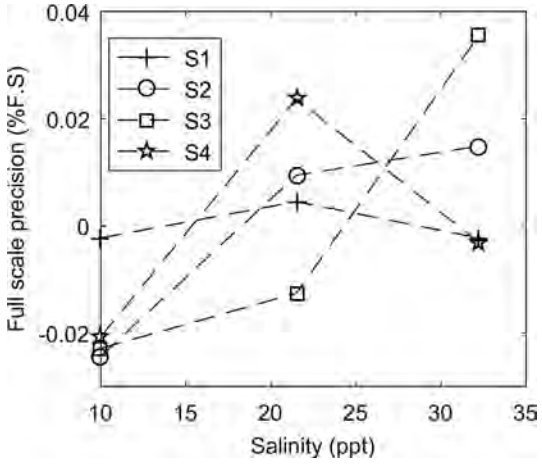

Fig. 9. Salinity effects of the measurements.

Table 2
Permission concentration of foreign ions for the determination of ammonia (under ± 5% error for 4 μ mol L^{-1} ammonia).

Coexisted ions	Permission concentration	Coexisted ions	Permission concentration
Cu^{2+}	258.3 $\mu g{\cdot}L^{-1}$	S^{2-}	696.9 $\mu g{\cdot}L^{-1}$
Fe^{3+}	1.2×10^4 $\mu g{\cdot}L^{-1}$	Br^-	1.92×10^6 $\mu g{\cdot}L^{-1}$
Hg^{2+}	1.0×10^4 $\mu g{\cdot}L^{-1}$	I^-	1.02×10^5 $\mu g{\cdot}L^{-1}$
NO_3^-	2.48×10^5 $\mu g{\cdot}L^{-1}$		

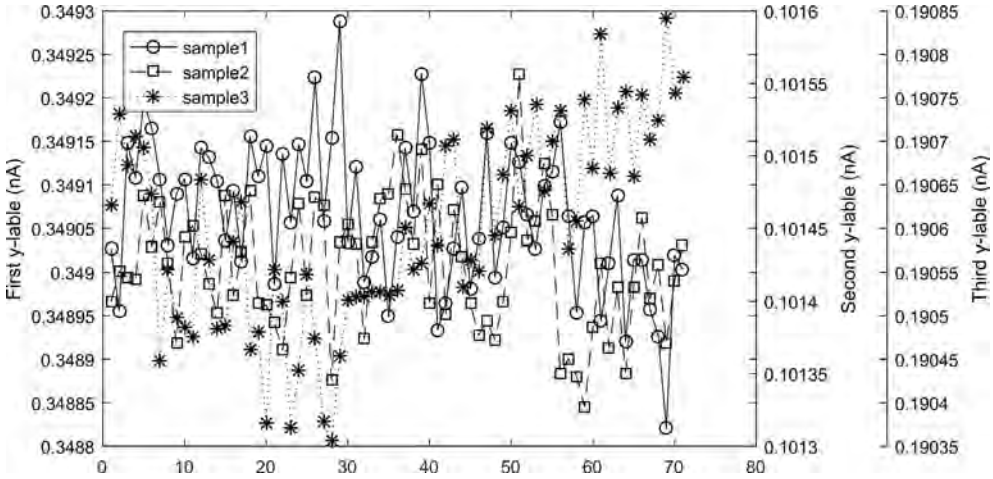

Fig. 8. Repeatability of the measurements.

Table 3
Accuracy analysis, $\mu g \cdot L^{-1}$. The underline values represent only the measured outliers.

Sample sources	H-readout	T-readout	Samples	H-readout	T-readout
Drinking water	0	9.37	Seawater	260	269.48
Fish tank water	80	79.89	Crab tank water	180	183.22
Aquaponics water	310	308.77	River water	850	419.31
Recirculating aquaculture water	190	196.56	Taihu Lake water	370	367.37

H-readout, this column of data was collected by Hach DR2800; T-readout, this column of data was collected by our transducer.

3.4.5. Accuracy analysis

Measurement accuracy reflects the closeness between the measurement result and the true value of the measurement. Accuracy is measured in error-the smaller the error, the higher the accuracy. In the laboratory, the ambient temperature was controlled at about 25 °C, and eight groups of samples were measured. The sample concentrations were checked using a commercial spectrophotometer, Hach DR2800 (Salicylate method: 20–2500 $\mu g \cdot L^{-1}$). Comparisons of the fluorometric transducer and salicylate method are listed in Table 3. There was one outlier in the river water sample. The likely possibility was that the ammonia concentration of the sample was outside the range of the sensor. As described in Fig. 10, in a wide range of ammonia concentrations, the model results were in agreement with the spectrophotometer data. The similarity of results demonstrated the comparability of the two methods.

3.4.6. Limit of detection, comparison with classical methods

Generally, limit of detection (LOD) refers to the ability of a measuring instrument to distinguish between the lowest quantity of a substance and the absence of that substance (a blank value). The detection limit is estimated from the mean of the blank, the standard deviation of the blank and some confidence factor. Another consideration that affects the detection limit is the accuracy of the model used to predict concentration from the raw analytical signal.

In our experiment, ten blank parallel samples were measured by the fluorometric transducer and the Low Detection Limit (LOD) was analyzed according to formula: $LOD = 3 \times S_b/S$ (Shrivastava and Gupta, 2011), where S_b is the standard deviation of the blank signal and S is the transducer calibration curve slope (S = 5.62). Table 4 shows the response voltage of measuring of the ten blank parallel samples. The LOD of the transducer is 0.16 $\mu g \cdot L^{-1}$.

Table 5 shows the comparison with sensors of other companies, and it indicates that our sensor had the advantage of being better sensitive and consistency for quantifying ultratrace ammonia nitrogen.

M1, OPA (Colorimetry); M2, Ion selective electrode; M3, Ammonia sensitive electrode; M4, Indophenol blue method; M5, OPA (Vertical scattering method)

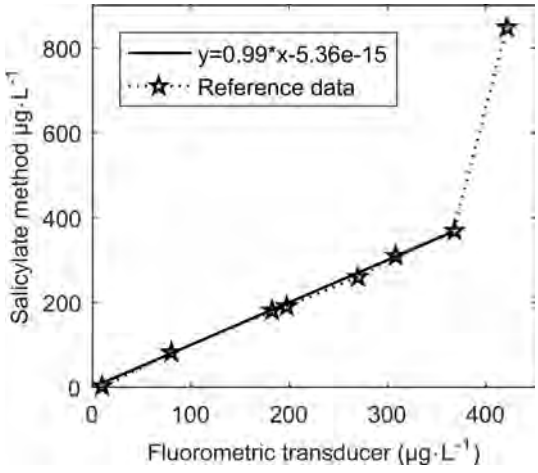

Fig. 10. Fluorometric transducer vs. salicylate method.

3.5. Calculation of unionized ammonia

In natural surface waters, ammonia nitrogen exists in two forms: unionized ammonia or free ammonia, NH_3, and ionized ammonia, NH_4^+. The well-known toxicity of ammonium salts to freshwater and marine life is caused by the unionized ammonia (NH_3), because it rapidly penetrates cell membranes via the lipoidal segments (Souza-Bastos et al., 2015). Some studies have quantified the percentage NH_3 in solution as a function of pH and temperature (Zhou, 2016; Boyd and Tucker, 2014). If NH_3 detection in an aquatic system requires high accuracy, the effect of salinity on the dissociation constant of ammonia must also be considered. The fluorometric transducer provides a concentration that is inclusive of two forms, total ammonia nitrogen (TAN) and NH_3. The percentage of NH_3 may also be computed using the Hampson and Whitfield expression (Hampson, 1977; Whitfield, 1974):

Freshwater.

$$\%NH_3 = 100[1 + anti\log(pK_a^0(T)(P) - pH)]^{-1}$$
$$= 100[1 + anti\log(18.915 - 0.0324T + 0.0415P/T - pH)]^{-1} \quad (9)$$

Sea water.

$$\%NH_3 = 100[1 + anti\log(pK_a^s(T)(P)(S) - pH)]^{-1}$$
$$= 100[1 + anti\log(-0.467 + 0.00113S + 2887.9/T + 0.0415P/T - pH)]^{-1} \quad (10)$$

$$NH3 = \%NH_3(NH_3 + NH_4^+) = \%NH_3 \times TAN \quad (11)$$

where T is the absolute temperature (K), P is the pressure (atm), S is the salinity (ppt), pK_a^0 is the acidic dissociation constant of ammonium ions at 298 K and zero ionic strength, pK_a^s is the stoichiometric acidic hydrolysis constant of ammonium ions in saline water, and the TAN value is directly obtained by the fluorometric transducer.

4. Conclusion

To detect ultra-low levels of aqueous ammonia nitrogen in natural waters, a highly sensitive optical transducer based on light intensity fluorometric detection has been designed. The advantages of the unique optical path with internal reference measurement have been highlighted and the unique photodiode-amplifier circuitry and synchronous demodulation have been described. A PRS modulation theory is successfully applied to measure the amplitude of the weak fluorescence signal, and careful selection of optoelectronic and electronic components has resulted in a very high signal-to-noise ratio and repeatability. A specially developed circuitry eliminates the influence of ambient light, which is normally present in surface waters. Benefiting from the temperature sensor installed on the back of the reference photodiode, the internal reference measurement of the emitted light compensates for aging and temperature dependencies of the high-efficiency LEDs used for fluorescence excitation. Moreover, this paper provides two sets of algorithms for calculating the content of the unionized ammonia, correcting for pH, temperature, salinity, and atmospheric pressure. The experiments showed that the transducer presents a high degree of

Table 4
The results of measuring of the ten blank parallel samples, mV.

Number	1	2	3	4	5	6	7	8	9	10
Results	128.52	128.99	128.09	128.08	127.96	128.33	128.35	128.14	128.25	128.49

Table 5
Comparison with the sensors of other companies.

Company	SYSTEA	S::CAN	WTW	HACH	Our sensor
Principle	M1	M2	M3	M4	M5
Ranges ($\mu g{\cdot}L^{-1}$)	0–1000	$0–10^6$	$0–10^6$	0–2000	0–419
Sensitivity ($\mu g{\cdot}L^{-1}$)	20	100	100	20	0.16
Consistency error	± 2%	± 3%	± 5%	± 4%	± 0.86%

linearity ($R^2 = 0.99$) within the concentration range of 0–419 $\mu g{\cdot}L^{-1}$. The limit of detection is 0.16 $\mu g{\cdot}L^{-1}$. The salinity in sea water was found to have little influence on the measurement system. This greatly enhances the universality of the fluorometric transducer.

Acknowledgments

The authors are grateful for financial support from the National Natural Science Foundation of China (Grant No. 61571444); the Key Research and Development Program of Shandong Province (Grant No. 2016CYJS03A02). We would like to thank Professor Zhong-li Pan for providing an English language edit of this article.

References

Akbarzadeh-Jahromi, S.A., Shahabadi, M., 2017. Low-cost highly sensitive refractive index measurement based on deep frequency modulation interferometry. IEEE Sens. J. 17 (17), 5460–5465.
Ardeniswan, D.F., Sukmawati, F., 2017. Acute toxicity of ammonia to carp fish (Cyprinus carpio) at different pH Levels. In: 1st International Symposium on Green Technology for Value Chains 2016, 60 (2017) 1–5.
Ben-Asher, R., Lahav, O., 2016. Electrooxidation for simultaneous ammonia control and disinfection in seawater recirculating aquaculture systems. Aquacult. Eng. 72–73 (2016), 77–87.
Boyd, C.E., Tucker, C.S., 2014. Handbook for Aquaculture Water Quality. Craftmaster Printers, Auburn, Alabama.
Bushaw, K.L., Zepp, R.G., Tarr, M.A., Schulz-Jander, D., Bourbonniere, R.A., Hodson, R.E., 1996. Photochemical release of biologically available nitrogen from aquatic dissolved organic matter. Nature 381 (6581), 404–407.
Cheng, X., Hou, L., Liu, M., Zheng, Y., Yin, G., Li, X., 2015. Inorganic nitrogen exchange across the sediment–water interface in the eastern chongming tidal flat of the yangtze estuary. Environ. Earth Sci. 74 (3), 2173–2184.
Cho, Y.B., Jeong, S.H., Chun, H., Kim, Y.S., 2018. Selective colorimetric detection of dissolved ammonia in water via modified Berthelot's reaction on porous paper. Sens. Actuat. B Chem. 256 (2018), 165–175.
Dahlberg, D., Ivanovic, J., Hassel, B., 2015. Toxic levels of ammonia in human brain abscess. J. Neurosurg. 124 (3), 1–7.
Ding, J., Zhao, Q.L., Jiang, J.Q., Wei, L.L., Wang, K., Zhang, Y.S., 2016. Electrochemical disinfection and removal of ammonia nitrogen for the reclamation of wastewater treatment plant effluent. Environ. Sci. Pollut. Res. Int. 24 (6), 1–7.
Eshchar, M., Lahav, O., Mozes, N., Peduel, A., Ron, B., 2006. Intensive fish culture at high ammonium and low ph. Aquaculture 255 (1–4), 301–313.
Guan, F., Hong, Y., Jiapeng, W.U., Wang, Y., Liying, B., Tang, B., 2017. A fast sodium hypobromite oxidation method for the sequential determination of ammonia nitrogen in small volume. Ecolog. Sci. 36 (2), 42–48.
Hampson, B.L., 1977. Relationship between total ammonia and free ammonia in terrestrial and ocean waters. ICES J. Mar. Sci. 37 (2), 117–122.
Hashihama, F., Kanda, J., Tauchi, A., Kodama, T., Saito, H., Furuya, K., 2015. Liquid waveguide spectrophotometric measurement of nanomolar ammonium in seawater based on the indophenol reaction with o-phenylphenol (OPP). Talanta 143 (2015), 374–380.
Hoang, P.H., Nguyen, H.T., Tran, T.T., 2017. Isolation and selection of nitrifying bacteria with high biofilm formation for treatment of ammonium polluted aquaculture water. J. Vietnamese Environ. 8 (1), 33–40.
Holmes, R.M., Aminot, A., Kérouel, R., Hooker, B.A., Peterson, B.J., 1999. A simple and precise method for measuring ammonium in marine and freshwater ecosystems. Can. J. Fish. Aquat. Sci. 56 (10), 1801–1808.
Hong, D.D., Rhee, J.I., 2014. A ratiometric fluorescence sensor for the detection of ammonia in water. Sens. Actuat. B Chem. 190 (1), 768–774.
Horstkotte, B., Duarte, C.M., Cerdà, V., 2011. A miniature and field-applicable multipumping flow analyzer for ammonium monitoring in seawater with fluorescence detection. Talanta 85 (2011), 380–385.
Hou, K., Yang, M., Qian, H., Lin, T., Panpan, X.U., 2017. The background values of ammonia-nitrogen, total phosphorus and cod of the mainstream of yellow river within Ningxia province. J. Irrigat. Drain. 36 (8), 65–71.
Hu, Y., Pan, Y., Sun, L., Chen, H., Jiang, K., Pan, J., 2013. An in-situ highly sensitive and reliable chlorophyll sensor based on pseudo-random sequence modulation. IEEE Trans. Instrum. Meas. 62 (8), 2314–2322.
Hu, Y., Sun, L., Ye, S., Chen, H., Jiang, K., Pan, J., 2014c. A highly sensitive in-situ, turbidity sensor with low power consumption. Photonic Sens. 4 (1), 77–85.
Hu, Y., Sun, L., Ye, S., Chen, H., Pan, J., Gao, X., 2014. A highly sensitive in-situ CDOM sensor. In: IEEE International Conference on Information and Automation, Yinchuan, 2013, pp. 648–652.
Hu, H., Ying, L., Li, S., Guo, Q., Wu, C., 2014a. A modifiedo-phthalaldehyde fluorometric analytical method for ultratrace ammonium in natural waters using EDTA-NaOH as buffer. J. Analyt. Meth. Chem. 2014 (4), 1–7.
Jiménez-Márquez, F., Vázquez, J., Sánchez-Rojas, J.L., 2015. Optoelectronic sensor device for monitoring the maceration of red wine: design issues and validation. Measurement 63 (2015), 128–136.
Johnson, M.T., Liss, P.S., Bell, T.G., Lesworth, T.J., Baker, A.R., Hind, A.J., 2008. Field observations of the ocean-atmosphere exchange of ammonia: fundamental importance of temperature as revealed by a comparison of high and low latitudes. Global Biogeochem. Cycles 22 (1), 1–15.
Kérouel, R., Aminot, A., 1997. Fluorometric determination of ammonia in sea and estuarine waters by direct segmented flow analysis. Mar. Chem. 57 (97), 265–275.
Kołacińska, K., Koncki, R., 2014. A novel optoelectronic detector and improved flow analysis procedure for ammonia determination with Nessler's Reagent. Analyt. Sci. Int. J. Japan Soc. Analyt. Chem. 30 (10), 1019–1022.
Li, X., Chen, H., Jiang, X., Yu, Z., Yao, Q., 2017. Impacts of human activities on nutrient transport in the yellow river: the role of the water-sediment regulation scheme. Sci. Total Environ. 592 (2017), 161–170.
Li, F., Wei, Y., Chen, Y., Li, D., Zhang, X., 2015. An intelligent optical dissolved oxygen measurement method based on a fluorescent quenching mechanism. Sensors. 15 (12), 30913–30926.
Liang, Y., Yan, C., Guo, Q., Xu, J., Hu, H., 2016. Spectrophotometric determination of ammonia nitrogen in water by flow injection analysis based on NH_3-o-phthalaldehyde-Na_2SO_3, reaction. Anal. Chem. Res. 10 (2016), 1–8.
Lich, N.Q., Kumar, M.S., 2017. Evaluation of mechanical methods used for the enhancement of dissolved oxygen and removal of ammonia toxicity from intensive shrimp farming wastewater. J. Eng. Comput. Appl. Sci. 6 (11), 26–41.
Lukin, K., Shcherbakov, V., 2016. New method for generation of binary pseudo-random sequences with quasiperfect autocorrelation. In: 9th International Kharkiv Symposium on Physics and Engineering of Microwaves, Millimeter and Submillimeter Waves, Kharkiv, Ukraine, 2016, pp. 1–5.
Ma, J., Adornato, L., Byrne, R.H., Yuan, D., 2014. Determination of nanomolar levels of nutrients in seawater. Trends Anal. Chem. 60 (2014), 1–15.
Matsui, M., Gotoh, T., Ishibashi, T., Nishikawa, M., 2010. Simultaneous determination of ammonia, nitrite and nitrate in the environmental samples by HPLC. J. Environ. Chem. 7 (1), 23–30.
Mayerhöfer, T.G., Mutschke, H., Popp, J., 2016. Employing theories far beyond their limits-the case of the (Boguer-)Beer-Lambert Law. Chemphyschem 17 (13), 1948–1955.
Mook, W.T., Chakrabarti, M.H., Aroua, M.K., Khan, G.M.A., Ali, B.S., Islam, M.S., 2012. Removal of total ammonia nitrogen (TAN), nitrate and total organic carbon (TOC) from aquaculture wastewater using electrochemical technology: a review. Desalination 285 (3), 1–13.
Mooney, T.J., Pease, C., Trenfield, M., Van, R.D., Harford, A.J., 2018. Modelling the Ph-ammonia toxicity relationship for hydra viridissima in soft-waters with low ionic concentrations. Environ. Toxicol. Chem. 37 (4), 1189–1196.
Mueller, A.V., Hemond, H.F., 2016. Statistical generation of training sets for measuring NO_3^-, NH_4^+ and major ions in natural waters using an ion selective electrode array. Environ. Sci. Process Impacts 18 (5), 590–599.
Naidji, B., Husson, J., Taouil, A.E., Brunol, E., Sanchez, J.B., Berger, F., 2016. Terpyridine-based metallopolymer thin films as active layer in ammonia sensor device. Synth. Met. 221 (2016), 214–219.
Ohira, S., Heima, M., Yamasaki, T., Tanaka, T., Koga, T., Toda, K., 2013. Flow-based ammonia gas analyzer with an open channel scrubber for indoor environments. Talanta 116 (2013), 527–534.
Pan, Y., Ye, S., Yang, J., Pan, J., Hu, Y., 2011. Fluorescence measurement system based on pseudo-random sequence modulation. Chin. J. Sci. Instrum. 32 (7), 1470–1477.
Rixen, T., Baum, A., Gaye, B., Nagel, B., 2014. Seasonal and interannual variations in the nitrogen cycle in the Arabian Sea. Biogeosci. Discuss. 10 (12), 19541–19570.
Roinila, T., Luhtala, R., Salpavaara, T., Verho, J., Messo, T., Vilkko, M., 2016. Rapid high-frequency measurements of electrical circuits by using frequency mixer and pseudo-random sequences. Modeling Identif. Control 37 (2), 113–119.
Shrivastava, A., Gupta, V.B., 2011. Methods for the determination of limit of detection and limit of quantitation of the analytical methods. Drug Discov. Therapeut. 2 (1),

21–25.
Souza-Bastos, L.R., Val, A.L., Wood, C.M., 2015. Are amazonian fish more sensitive to ammonia? toxicity of ammonia to eleven native species. Hydrobiologia 789 (1), 1–13.
Šraj, L.O., Almeida, M.I.G.S., Swearer, S.E., Kolev, S.D., Mckelvie, I.D., 2014. Analytical challenges and advantages of using flow-based methodologies for ammonia determination in estuarine and marine waters. Trac Trends Analyt. Chem. 59 (2014), 83–92.
Strobl, M., Walcher, A., Mayr, T., Klimant, I., Borisov, S.M., 2017. Trace ammonia sensors based on fluorescent near-infrared-emitting aza-BODIPY dyes. Anal. Chem. 89 (5), 2859–2865.
Valente, I.M., Oliveira, H.M., Vaz, C.D., Rui, M.R., Fonseca, A.J.M., Cabrita, A.R.J., 2017. Determination of ammonia nitrogen in solid and liquid high-complex matrices using one-step gas-diffusion microextraction and fluorimetric detection. Talanta 167 (2017), 747–753.
Whitfield, M., 1974. The hydrolysis of ammonium ions in sea water-a theoretical study. J. Mar. Biol. Assoc. UK 54 (3), 565–580.
Xin, Y., He, G., Wang, Q., Yu, F., 2011. A portable fluorescence detector for fast ultra trace detection of explosive vapors. Rev. Sci. Instrum. 82 (10), 103102 (1–8).
Yan, C.M., Liu, X., Liang, Y., Yin, S.M., 2015. Determination of ammonia nitrogen in natural water sample using solid-phase fluorescence spectrometry based on OPA-NH_3-sulfite reaction. J. Instrum. Anal. 34 (11), 1271–1275.
Yang, Y.M., Lou, K.K., Zhou, L.C., Ye, S.M., 2010. Design of a high-sensitivity, low-power instrument for chlorophyll a measurements. Int. Conf. Biomed. Eng. Inform. 4 (1), 1450–1454.
Yu, H., Ding, L., Liu, S.W., Ding, J.W., Qin, W., 2017. Research progress on determination of ammonia nitrogen in seawater. Chem. Bioeng. 34 (5), 1–7.
Zeng, Y.G., Chen, L., Li, H.X., Huang, J., Yu, B., 2014. Comparison study on measuring ammonia and nitrogen in surface water by flow injection and Nessler's Reagent. Adv. Mater. Res. 884–885 (2014), 46–50.
Zhang, T., 2017. Effect of ammonia nitrogen content in raw water on chlorine consumption. Petrochem. Indus. Technol. 1 (2017), 1–6.
Zhang, H., Gu, L., Liu, B., Gan, H., Zhang, K., Jin, H., 2016. An improved biofilter to control the dissolved organic nitrogen concentration during drinking water treatment. Environ. Sci. Pollut. Res. 23 (18), 1–8.
Zhang, F., Wei, Y., Chen, Y., Liu, C., 2014. Intelligent ammonia-nitrogen sensor which based on ammonia electrode. IFIP Adv. Inform. Commun. Technol. 420 (2014), 534–543.
Zhang, L., Xu, E.G., Li, Y., Liu, H., Vidal-Dorsch, D.E., Giesy, J.P., 2018. Ecological risks posed by ammonia nitrogen (AN) and un-ionized ammonia (NH_3) in seven major river systems of china. Chemosphere 202 (2018), 136–144.
Zhang, B.R., Zheng, D.Z., Sun, C.W., Rong-Jin, Y.U., 2009. The detection of weak light signal based on pseudo-random sequences. Acta Electron. Sin. 37 (9), 2082–2084.
Zhou, L., 2016. Comparison of nessler, phenate, salicylate and ion selective electrode procedures for determination of total ammonia nitrogen in aquaculture. Aquaculture 450 (1), 187–193.
Zhou, L., Boyd, C.E., 2015. An assessment of total ammonia nitrogen concentration in alabama (USA) ictalurid catfish ponds and the possible risk of ammonia toxicity. Aquaculture 437 (2015), 263–269.
Zhu, Y., Yuan, D., Huang, Y., Ma, J., Feng, S., Lin, K., 2014. A modified method for on-line determination of trace ammonium in seawater with a long-path liquid waveguide capillary cell and spectrophotometric detection. Mar. Chem. 162 (2014), 114–121.